Frequency drift of Saturn chorus emission compared to nonlinear theory

J. D. Menietti,[1] Y. Katoh,[2] G. B. Hospodarsky,[1] and D. A. Gurnett[1]

Received 23 October 2012; revised 31 January 2013; accepted 1 February 2013; published 20 March 2013.

[1] The fine structure of nonlinear drifting-frequency chorus is observed at Saturn by the Cassini Radio and Plasma Wave Investigation. During a high-inclination orbit in which Cassini is at near-constant L-shell within about 10° of the magnetic equator, moderately intense nonlinear chorus is observed. Cassini observed a region of intense chorus and large bandwidth a few degrees on either side of the magnetic equator, with lower intensities and bandwidths observed nearest the magnetic equator. Using the observed plasma wave spectra and electron phase space distribution, we have measured plasma parameters within or near the chorus generation region and evaluated the theoretical value of the frequency sweep rate, $\partial f/\partial t$, based on the nonlinear wave growth theory of Omura et al. and the backward wave oscillator theory of Trakhtengerts. Both theories produce rates that are within a factor of 2 of the observed values, but the nonlinear wave growth theory values are closer to the observations for the cases examined. The work presented is consistent with nonlinear theory in the generation of chorus, but also reveals a distinct region of weaker or linear chorus growth nearest to the magnetic equator at Saturn.

Citation: Menietti, J. D., Y. Katoh, G. B. Hospodarsky, and D. A. Gurnett (2013), Frequency drift of Saturn chorus emission compared to nonlinear theory, *J. Geophys. Res. Space Physics*, *118*, 982–990, doi:10.1002/jgra.50165.

1. Introduction

[2] There are two general types of whistler-mode emission present in planetary magnetospheres: hiss and chorus. Whistler mode emission exists at frequencies less than either the plasma frequency, f_p, or the cyclotron frequency, f_c, whichever is lower, but in the inner magnetospheric region $f_p > f_c$. Hiss has a featureless spectrum and is typically at lower frequencies than chorus, which often has a banded structure and, at high resolution, displays a fine structure of many frequency-drifting tones or chirps that have larger than typical spectral densities. These structures are the result of the nonlinear nature of chorus and resonant wave trapping of electrons as described, for instance, by *Nunn et al*. [1997], *Trakhtengerts et al*. [1996], *Trakhtengerts* [1999], *Omura and Summers* [2004, 2006], and *Katoh and Omura* [2004, 2006a, 2006b, 2007a, 2007b, 2011]. *Omura et al*. [2007] have extended the work of *Omura and Summers* [2006] to describe an extremely efficient nonlinear mechanism for accelerating high-energy electrons (seed electrons of approximately several hundred kiloelectron-volts) to a few megaelectron-volts in only a few seconds. This process, which the authors call relativistic turning acceleration, requires relatively large amplitude chorus emissions and an initial population of mildly energetic electrons. *Summers and Omura* [2007] described an ultrarelativistic acceleration mechanism for electrons that is possible at Jupiter and other planetary magnetospheres. This mechanism involves nonlinear trapping of electrons by coherent whistler-mode waves. *Summers and Omura* [2007] proposed that under ideal conditions at Jupiter near $L = 8$, several hundred kiloelectron-volt electrons can be energized by tens of megaelectron-volts in a few tens of seconds. The electrons undergoing ultrarelativistic acceleration would have previously been accelerated by the process of relativistic turning acceleration [*Omura et al*., 2007] or by other processes. *Bortnik et al*. [2008] have performed test-particle modeling for oblique waves as well, finding that nonlinear phase-trapping leads to rapid, large increase in energy and pitch-angle for a small fraction of test-particles.

[3] *Omura et al*. [2008, 2009] described the nonlinear process of frequency dispersion (i.e., frequency drifting) of whistler-mode chorus elements. This theoretical dispersion can be calculated from measured local parameters and compared to measured frequency dispersion of chorus elements when high-resolution wave data are available. Specifically, *Omura et al*. [2008] described the frequency dispersion of whistler-mode chorus by their equation (50), which expresses $\partial\omega/\partial t$ in terms of wave frequency, local cyclotron frequency, local plasma frequency, wave magnetic field amplitude, parallel velocity of the electrons, and temperature anisotropy of the electron distribution. All of these parameters are often available from the plasma wave data measured by the Cassini radio and plasma wave science (RPWS) instrument, and the electron phase space distribution function derived from the Cassini electron spectrometer (ELS). By

[1]University of Iowa, Department of Physics and Astronomy, Iowa City, Iowa, USA.
[2]Tohoku University, Department of Geophysics, Graduate School of Science, Sendai, Japan.

Corresponding author: J. D. Menietti, The University of Iowa, 210 Van Allen Hall, University of Iowa, Iowa City, IA 52242–1479, USA. (john-menietti@uiowa.edu)

2169-9380/13/10.1002/jgra.50165

calculating $\partial\omega/\partial t$ from the measured local parameters, a theoretical value can be obtained that can be directly compared to the measured frequency dispersion or drift rate.

[4] *Trakhtengerts* [1999] has described a nonlinear theory of chorus growth referred to as the backward wave oscillator (BWO). In this theory as applied to magnetospheric space physics, a step-like distribution function, which is formed by cyclotron interactions of energetic electrons of the whistler mode hiss (ELF/VLF noise-like emissions) is necessary [*Trakhtengerts et al*., 1996]. It is this distribution that yields the large growth rate of the whistler mode waves and development of the absolute cyclotron instability in a narrow region near the equatorial plane. *Titova et al*. [2012] have simplified the expression for frequency sweep rate of chorus in terms of the trapping frequency, described later, and parameters that are readily measurable (their equation (1)).

[5] Several recent observational studies of terrestrial nonlinear chorus have investigated a range of issues. *Macusova et al*. [2010] have performed a statistical study of frequency sweep rates using Cluster chorus emission data. They found increasing values of the sweep rate for decreasing plasma densities, in agreement predictions of the BWO theory. *Cully et al*. [2011] used observations by the THEMIS Spacecraft and demonstrated that frequency drift rates agreed with predictions of *Omura et al*. [2008] based on wave amplitude. The authors measure the phase space distribution near the chorus source region and then compare the expected sweep rate to that observed. *Tao et al*. [2012], using chorus emission observed by the THEMIS satellites, found that frequency sweep rates predicted by *Helliwell* [1967] and the BWO theory agree with observations as a function of magnetic local time and geomagnetic activity.

[6] *Santolik et al*. [2003] presented high-resolution Cluster satellite observations of the terrestrial chorus source region that indicated a dimension of a few thousand kilometers along the magnetic field line. Their studies suggest a region of exponential electric field growth phase, which could be consistent with a linear instability, but also with probable nonlinear magnetic field fluctuations. More recently, *Santolik et al*. [2009] presented Cluster high-resolution plasma wave observations that show evidence that the intensity of nonlinear chorus emissions very near the magnetic equator increase with distance along the field line away from the equator. These authors state this is consistent with an extended source region of several thousand kilometers centered at the magnetic equator with chorus gradually amplified away from the equator but well within the source region.

[7] *Hospodarsky et al*. [2008] have reported a survey of chorus emissions at Saturn describing probable source regions, typical amplitudes, and some of the similarities and differences of this ubiquitous emission relative to terrestrial observations, including the presence of nonlinear drifting-frequency structures. *Hospodarsky et al*. [2012] and *Menietti et al*. [2012] have more recently extended these studies by comparison with Jovian chorus emissions as well. Calculations of linear chorus growth rates based on in situ plasma and wave observations have been reported by *Menietti et al*. [2008a, 2008b], indicating measurable temperature anisotropies in the electron phase space distribution.

[8] In this present paper, we will examine chorus emission observed by the Cassini spacecraft near the magnetic equator during a high-inclination orbit. The observations show a similarity to those of *Santolik et al*. [2009]. The data present nonlinear drifting-frequency chorus structures that can be measured and compared to theory of both *Omura et al*. [2008] and *Trakhtengerts* [1999].

2. Observations and Theory

[9] Figure 1 is an example of chorus emission observed by the RPWS magnetic field search coils on board Cassini

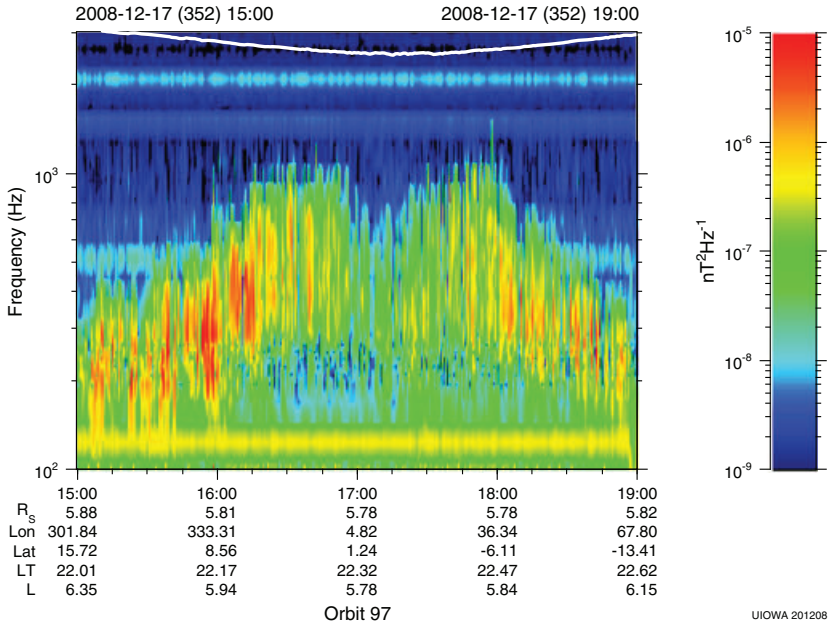

Figure 1. A frequency-time spectrogram with magnetic field spectral density color-coded. The chorus data are from the low-rate receiver of the RPWS during an equator crossing at near-constant L-shell. Note the decrease in chorus bandwidth and intensity near the magnetic equator crossing (~17:00 to ~17:20). The white line displays the local cyclotron frequency.

during a high-inclination orbit when the spacecraft crossed the equator from north to south at near-constant L-shell. This plot shows rather intense chorus emission at frequencies less than the cyclotron frequency. Within about 2° of the magnetic equator, the chorus emission intensity and bandwidth decreases with the lowest intensity observed closest to the magnetic equator near 17:10. *Santolik et al*. [2009] made reference to this effect for terrestrial chorus as mentioned earlier. Not seen in this figure are higher-frequency signatures that appear as frequency-drifting features and are interpreted as nonlinear fine structures. In Figure 2a, we show a higher resolution plot of these signatures obtained from the Cassini Wideband receiver (WBR), which measures only electric field intensity on one of the three available antennas. The frequency dispersion of the waves is seen as broad-banded fine structures extending to higher frequency. These features are absent nearest the magnetic equator and extend to higher frequency and larger bandwidth with increasing latitude, peaking near ±5 to 6°. Note the broadband spikes nearest the magnetic equator are electrostatic bursts, possibly related to electron beams seen associated with this time. The RPWS also includes a 5-channel (2 electric and 3 magnetic) Waveform Receiver (WFR) which measures waveforms up to 2.5 kHz in 140 μs snapshots approximately every 5 min. In Figure 2b we plot a spectrogram of the three WFR axial magnetic search coils for the time period 15:45 to 18:30. The data for each snapshot are "blended" over the approximately 5 min intervening interval. These data provide accurate determination of the magnetic field magnitude, B_w, during the snapshot, but do not reveal frequency dispersion.

[10] In Figures 3a–3c we show spectrograms of WBR electric field data at even higher resolution featuring three drifting-frequency signatures observed in the data at various times. We have calculated the frequency dispersion with a least-squares fit to a line and find the respective dispersions, $\partial f/\partial t$, are 249 Hz/s, σ =72 Hz/s; 231 Hz/s, σ =70 Hz/s; and

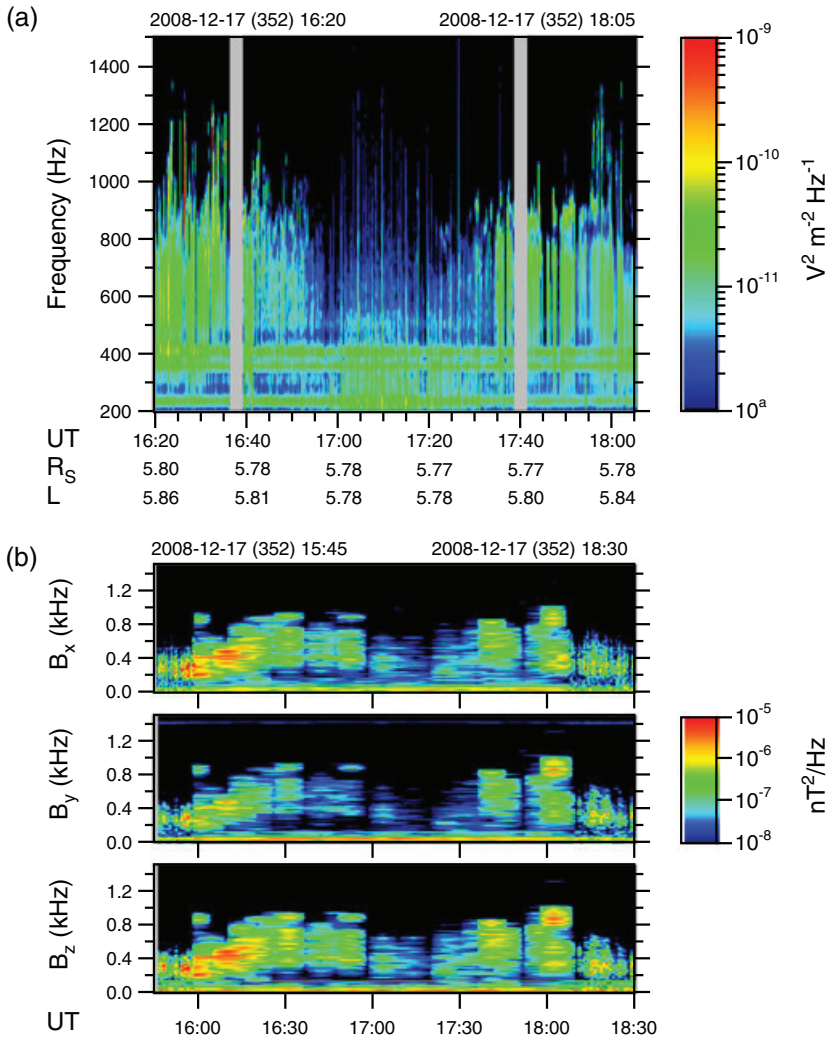

Figure 2. (a) A higher resolution spectrogram of the electric field spectral density obtained by the wideband receiver (WBR) for the same pass as Figure 1. Discrete nonlinear chorus features, which extend to higher frequencies, are seen a few degrees away from the magnetic equator. (b) A spectrogram of the three WFR axial magnetic search coils for the time period 15:45 to 18:30. The data for each snapshot are "blended" over the approximately 5 min intervening interval. These data provide accurate determination of the magnetic field magnitude, B_w, during the snapshot, but do not reveal frequency dispersion.

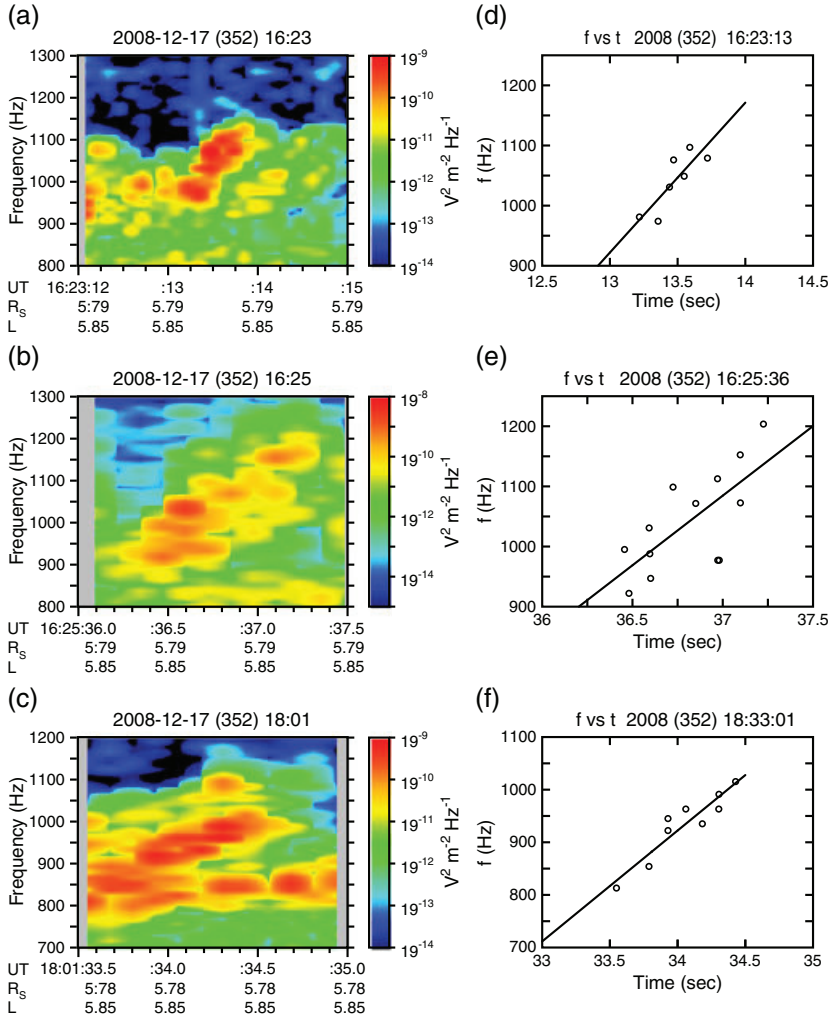

Figure 3. High-resolution electric field WBR spectrograms each taken during a nonlinear frequency-drifting event during time intervals (a) 16:23:12–15, (b) 16:25:36–37.5, and (c) 18:01:33–35. (e, f, and g) The least-squares fit to the corresponding data from Figures 3a, 3b, and 3c.

211 Hz/s, $\sigma = 28$ Hz/s, respectively. The fitted points used in the calculation of the slope are plotted in Figures 3d–3f. These points were selected manually directly from the plots using the crosshair function of the plotting tool. The standard deviation, σ for the slope was calculated according to the theory of error estimation [*Bevington*, 1969] assuming the standard deviation of each of the points is equal.

[11] To determine the theoretical nonlinear frequency drift $\partial\omega/\partial t$, we use the results of *Omura et al*. [2008]. These authors have defined the parameter S, the inhomogeneity factor as

$$S = -\frac{1}{\omega_t^2 \delta^2}\left\{\gamma\left(1-\frac{v_R}{v_g}\right)^2\frac{\partial\omega}{\partial t} + \left[\frac{k\gamma v_\perp^2}{2\Omega_e} - \left(1+\frac{\delta^2(\Omega_e-\gamma\omega)}{2(\Omega_e-\omega)}\right)v_R\right]\frac{\partial\Omega_e}{\partial h}\right\} \quad (1)$$

where h is the distance along the magnetic field from the magnetic equator, the assumed source region of the chorus emission, ω is the frequency, k is the wave number, c is the speed of light, Ω_e is the electron cyclotron frequency, $v_\perp$ is the average velocity of the distribution perpendicular to the magnetic field near the source region, $\omega_t = \sqrt{kv_\perp\Omega_\omega}$, $\Omega_\omega = eB_w/m_e$, B_w is the wave magnetic field, and m_e is the electron mass. Following *Omura et al*. [2008], near the magnetic equator we assume $\Omega_e = \Omega_{eo}(1+ah^2)$ with $\Omega_{eo} = \Omega_e$ at the equator, $a = 4.5/(L\,R_s)^2$, L is the magnetic L-shell, and R_s is the radius of Saturn. For chorus source regions very near the magnetic equator, $\partial\Omega_e/\partial h = 0$. As discussed by *Omura et al*. [2008] when $S \sim -0.4$ we expect electron trapping in chorus wave potentials and maximum nonlinear wave growth. *Omura et al*. [2008] then obtain

$$\frac{\partial\omega}{\partial t} = \frac{0.4\delta}{\gamma\xi}\frac{v_\perp}{c}\frac{\omega}{\Omega_e}\left(1-\frac{v_R}{v_g}\right)^{-2}\frac{B_w}{B_0}\Omega_e^2 \quad (2)$$

where B_0 is the ambient magnetic field,

$$\delta^2 = 1 - \frac{\omega^2}{c^2k^2}$$

$$\xi^2 = \frac{\omega(\Omega_e-\omega)}{\omega_{pe}^2}$$

$$\gamma = \left[1 - \frac{\left(v_\parallel^2 + v_\perp^2\right)}{c^2}\right]^{-1/2}$$

$$v_R = \frac{1}{k}\left(\omega - \frac{\Omega_e}{\gamma}\right)$$

$$v_g = \frac{c\xi}{\delta}\left[\xi^2 + \frac{\Omega_e}{2(\Omega_e - \omega)}\right]^{-1}$$

where ω_{pe} is the electron plasma frequency.

[12] Only weak (linear) chorus emission is observed closest to the magnetic equator, while strong nonlinear drifting frequency signatures appear a few degrees above and below the equator. We therefore solve equation (1) for the case $\partial\Omega_e/\partial h \neq 0$ to obtain

$$\frac{\partial\omega}{\partial t} = \frac{1}{s_1}\{-s_0\omega\Omega_\omega S - cs_2(2a\Omega_{eo}h)\} \quad (3)$$

where following *Omura et al*. [2009],

$$s_0 = \frac{\delta}{\xi}\frac{v_\perp}{c}$$

$$s_1 = \gamma\left(1 - \frac{v_R}{v_g}\right)^2$$

$$s_2 = \frac{1}{2\xi\delta}\left\{\frac{\gamma\omega}{\Omega_e}\left(\frac{v_\perp}{c}\right)^2 - \left[2 + \Lambda\frac{\delta^2(\Omega_e - \gamma\omega)}{\Omega_e - \omega}\right]\frac{v_R v_p}{c^2}\right\}$$

with $\Lambda = \omega/\Omega_e$, and $v_p = \omega/k$.

[13] To solve equation (3), we must know ω_{pe} and Ω_e as well as the phase space distribution of the electrons near the chorus source region. During the time of Figure 1 there is a strong signature of electrostatic upper hybrid resonance, $f_{uh} = \sqrt{f_p^2 + f_c^2}$, in a narrow band near 40 kHz (not shown) from which ω_{pe} can be obtained. We also have access to the electron particle distribution from the Cassini ELS instrument. In Figure 4, we show a plot of the 2-D contour of the logarithm (base 10) of the electron phase space distribution function $f(v)$ during the time of Figure 3a. We have performed a nonlinear fit of the electron phase space distribution assuming a bi-Maxwellian form (cf. equation (1), *Menietti et al*. [2008a, 2008b]). The parameters for each plasma component of the fit include the parallel thermal velocity, $v_\parallel$, and $T_\perp/T_\parallel$, from which we then obtain $v_\perp = v_\parallel\sqrt{T_\perp/T_\parallel}$ used in the evaluation of s_0 and s_2 needed to evaluate equation (3). The complete bi-Maxwellian fitting function was the sum of the four electron plasma populations and an additional cold ion background for charge neutrality. In Table 1 we list fitting parameters for each electron plasma component (n is the number density). The free-energy source of the chorus is the highest energy component. Also in Table 1 are the fitting parameters for the plasma distribution observed near the magnetic equator (t = 17:10:11).

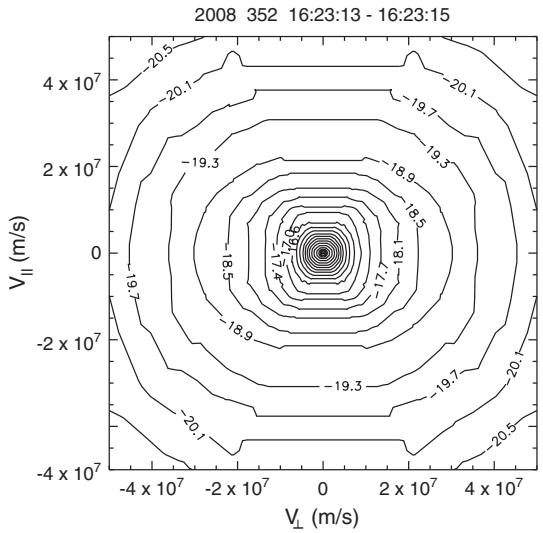

Figure 4. A two-dimensional contour of the $\log_{10}$ of the electron phase-space distribution in velocity space (s^3/m^6) for the time interval including that of Figure 3a.

[14] To obtain B_w, we utilize data from the WBR receiver and the high-resolution WFR data. The high-resolution electric field WBR data are available continuously at this time period, but is available from only one electric antenna. We use these data to indicate the location of the drifting signatures in frequency and time. WFR data, however, is available at high resolution from all three of the axial magnetic search coils, and thus provides an accurate value of B_w, but only operates in snapshots once each ~5 min. It is clear from Figure 2 that some of the most intense emission occurs during the periods of nonlinear frequency drift. A snapshot of WFR data obtained nearest the time period of Figures 3a and 3b at frequencies including those observed occurred at 16:30:53. At this time the intensity levels observed in the electric field are not as intense as those seen in Figures 3a and 3b. The bursty, drifting-frequency signatures are well fit by a straight line. Because we do not have measurements of B_w during the exact times and frequencies of Figures 3a–3c, we have used an average value of B_w over a range of frequencies. We chose a frequency range from the WFR data at nearby times that contained intense emission that overlapped a portion of the frequency range of the nonlinear features of Figure 3. At 16:30:53 the average value of $B_w = (B_w)_{obs} = 3.19\times10^{-3}$ nT for channels in the range 886 Hz $< f <$ 905 Hz observed during the WFR snapshot. Similarly, we determine the average value of $B_w = (B_w)_{obs} = 5.77\times10^{-3}$ nT for the drifting feature of Figure 3c using a WFR snapshot at time 18:01:33 for the channel range 847 Hz $< f <$ 869 Hz. In Table 2 we list some plasma parameters, observed values of $\partial f/\partial t$ fit to a straight line, $(\partial f/\partial t)_{obs}$, calculations of $(\partial f/\partial t)_O$ using equation (3) (based on the nonlinear wave growth theory), and calculations of $(\partial f/\partial t)_{Tr}$ using equation (4) (based on the BWO theory). The frequency sweep rates are evaluated for the examples of nonlinear drifting-frequency signatures of Figure 3, which all

Table 1. Phase Space Distribution Fitting Parameters

Event time	Plasma Component	n(m^{-3})	$v_\parallel$(m/s)	$T_\perp/T_\parallel$
16:23:13	cold core	1.83×10^7	1.33×10^5	1.0
	warm 1	3.76×10^6	1.73×10^6	1.17
	warm 2	2.44×10^5	5.52×10^6	0.833
	warm 3*	5.15×10^4	1.86×10^7	1.42
17:10:11	cold core	2.69×10^7	1.33×10^5	1.0
	warm 1	1.30×10^7	2.10×10^6	1.19
	warm 2	1.90×10^5	9.44×10^6	1.08
	warm 3*	2.54×10^4	3.60×10^7	1.33

*Chorus free energy source.

Table 2. $\partial f/\partial t$ for 2008/352

Event Time	f_c (Hz)	f_{uh} (Hz)	B_w (nT)	$v_{\|}$ (m/s)	$T_\perp/T_{\|}$	$\partial f/\partial t_{obs}$ (Hz/s)	$\partial f/\partial t_O$ (Hz/s)	$\partial f/\partial t_{Tr}$ (Hz/s)
16:23:13	2692	42,500	3.2×10^{-3}	1.84×10^{7}	1.42	249	58(150[b])	32(64[b])
16:25:36	2692	42,500	3.2×10^{-3}	1.86×10^{7}	1.42	231	61(154[b])	32(64[b])
18:01:33	2647	42,150	5.8×10^{-3}	1.84×10^{7}	1.42	211	144	62
17:10:11[a]	2563	57,000	1.9×10^{-4}	3.55×10^{7}	1.35	-	NA	NA

Subscripts: "obs" = observed; "O" = *Omura et al*. [2008]; "Tr" = *Trakhtengerts* [1999].
B_w = observed wave amplitude.
[a]Near magnetic equator.
[b]Evaluated at $B_w = 2(B_w)_{obs}$.

occur a few degrees away from the magnetic equator. The calculated values of $\partial f/\partial t$ are given for $f = 1$ kHz and at $(B_w)_{obs}$, and at $2(B_w)_{obs}$. The magnetic equator is encountered by Cassini near 17:10 where the intensity of the observed chorus is lower and the bandwidth smaller, and no nonlinear growth (defined by narrow-banded, frequency-drifting features) is observed. Row 4 of Table 2 lists the plasma parameters for the time near the crossing of the magnetic equator.

[15] To show the influence of the uncertainty in the measured values of the plasma parameters, in Figure 5 we plot $(\partial f/\partial t)_O$, as determined from equation (3) versus frequency for a range of values of the parameter B_w. The plots correspond to the chorus signatures at times 16:23:13 (Figure 5a), 16:25:36 (5b), and 18:01:33 (5c). In Figure 6 we plot $(\partial f/\partial t)_O$ versus B_w

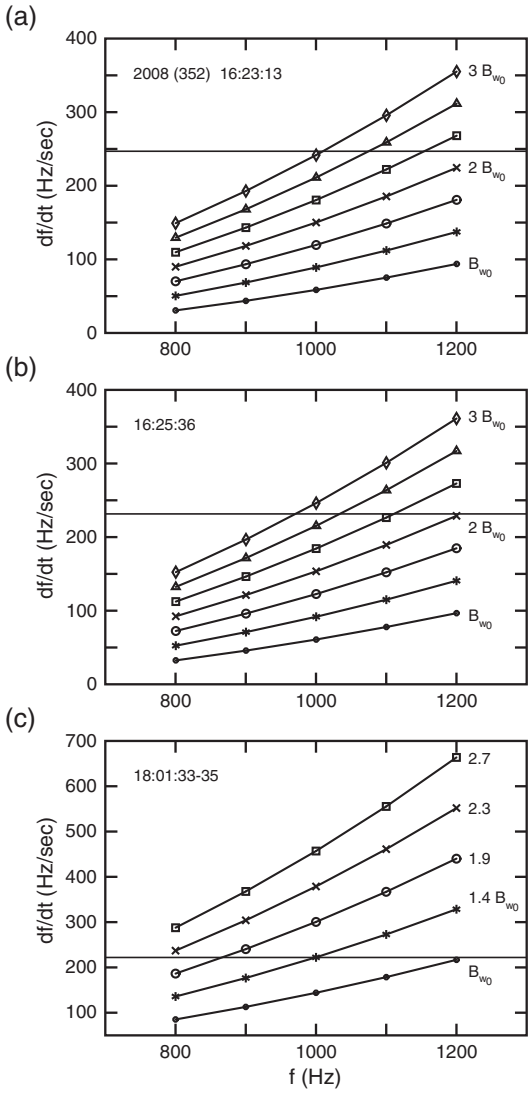

Figure 5. Model frequency drift rate versus frequency as determined from equation (3) for the time intervals of Figure 3 as displayed. The horizontal line in each panel indicates $(\partial f/\partial t)_{obs}$. (a and b) $B_{w0} = 3\times10^{-3}$ nT and (c) $B_{w0} = 5.77\times10^{-3}$ nT.

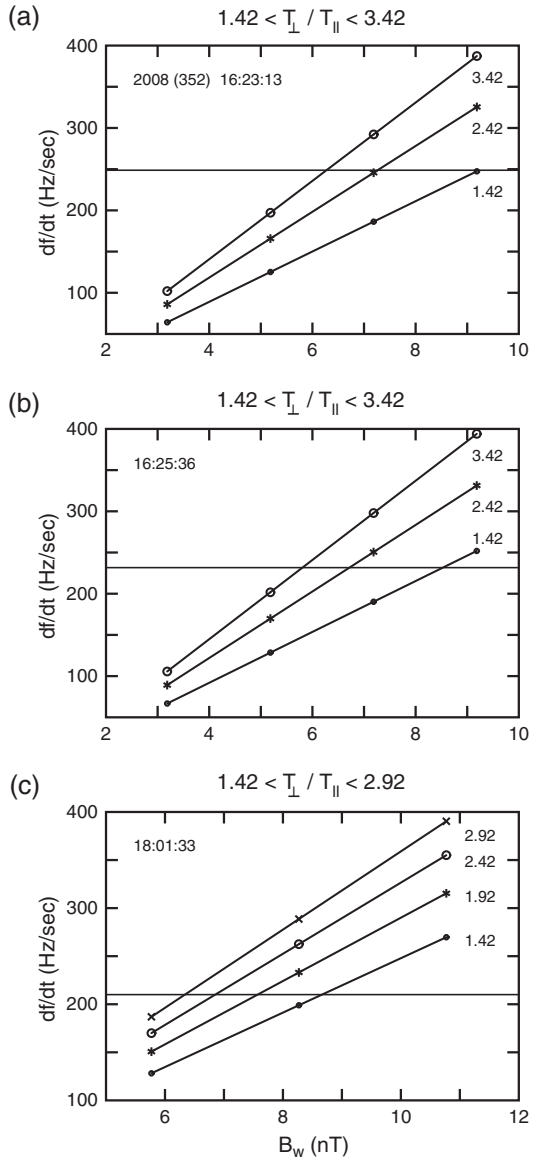

Figure 6. Model frequency drift rate versus B_w for the indicated time intervals of Figure 3 for a range of $T_\perp/T_{||}$ as shown. The horizontal line in each panel indicates $(\partial f/\partial t)_{obs}$.

for a range of values of $T_\perp/T_\parallel$ for the same three times (Figures 6a–6c). The parameters B_w and $T_\perp/T_\parallel$ have significant impact on the calculated value of $(\partial f/\partial t)_O$. A factor of 2 or 3 variation in the value of B_w is possible due to both temporal and spatial effects, because the WFR data used to make the estimates were not obtained simultaneously with the measurement of the drifting signature. It is apparent that varying B_w by a factor of 3 is enough to bring the calculated values of $\partial f/\partial t$ close to the measured values. Values of $(\partial f/\partial t)_{obs}$ ~200–250 Hz/s (observed values) are possible within a reasonable range of either/both B_w and $T_\perp/T_\parallel$, i.e., for $B_w < 8\times10^{-3}$nT ($B_w < 1.1\times10^{-2}$ nT for Figure 3c) and $T_\perp/T_\parallel \lesssim 2.4$.

[16] The plasma distribution was available for times 16:23:13–14 and for 16:25:36–37, but not for 18:01:33. We have assumed that the phase space distribution for the electrons near 18:01:33 is similar to that near 16:23:13, which lies nearly along the same L-shell, but on the other side of the magnetic equator. The ELS, which provides the data for the calculation of the phase space distribution, has an energy resolution of $\Delta E/E \sim 16.75\%$ and an angular resolution of 5 × 20 degrees. The measurement of the electron phase space distribution occurred over a 2 s sampling period, during which the distribution may have experienced relaxation because of the rapid growth of the chorus waves. Hence, we do not think it unreasonable to assume that actual values of $T_\perp/T_\parallel$ may be higher than the fitted values. *Menietti et al*. [2008a] estimated the value of $T_\perp/T_\parallel \sim 3$ or 4 would be necessary to produce sufficient chorus linear growth rate near the Saturn magnetic equator to match the observations of chorus wave amplitude, even though the observed (fitted) values were $T_\perp/T_\parallel \sim 1.5$ (similar to values found in the present cases). At Earth, *Santolik et al*. [2010] find ratios $T_\perp/T_\parallel > 10$ in the equatorial region where chorus is expected to be generated.

[17] We have also compared the data to the nonlinear BWO theory of *Trakhtengerts* [1999] and *Trakhtengerts et al*. [2004] as

$$(\partial f/\partial t)_{Tr} = \omega_t^2/(2\pi)^2 \quad (4)$$

where, as before, $\omega_t = \sqrt{\left(k\, V_\perp \Omega_c B'_w\right)}$ and $B'_w = B_w/B_0$. The values of $(\partial f/\partial t)_{Tr}$ evaluated from equation (4) are smaller than those derived from equation (3). We have included the results of the calculations for the measured parameters in column 9 of Table 1. In Figure 7 we plot $(\partial f/\partial t)_{Tr}$ versus f for a range of B_w and $T_\perp/T_\parallel$ for comparison with Figures 5a and 5c. We have omitted the event of 16:25:36 because it is quite similar to that of 16:23:13. We see that $(\partial f/\partial t)_{Tr}$ never reaches the observed value of 211 Hz/s for the range of plasma parameters shown. In Figure 8 we plot $(\partial f/\partial t)_{Tr}$ versus $T_\perp/T_\parallel$ for comparison with Figures 6a and 6c. Figure 8 shows that the values of $(\partial f/\partial t)_{Tr}$ approach the observed values for the parameters B_w and $T_\perp/T_\parallel$ at the maximum chosen limits $B_w \sim 3(B_w)_{obs}$ and $T_\perp/T_\parallel \sim 3(T_\perp/T_\parallel)_{obs}$.

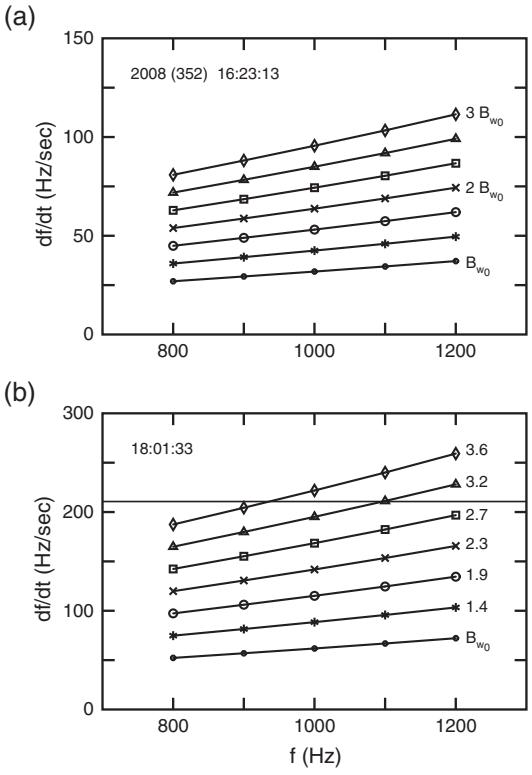

Figure 7. The format of this plot is the same as Figures 5a and 5c (and should be compared to them), but now the frequency drift rate is evaluated using equation (4) [*Trakhtengerts et al*., 2004]. (a) $B_{w0} = 10^{-3}$ nT and (b) $B_{w0} = 5.77 \times 10^{-3}$ nT. The horizontal line in Figure 7b indicates $(\partial f/\partial t)_{obs}$ for this time.

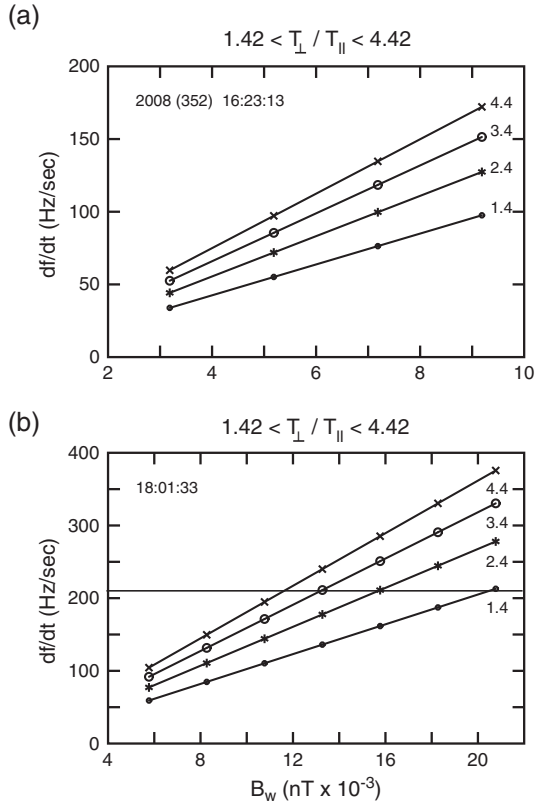

Figure 8. The format of this plot is the same as Figures 6a and 6c (and should be compared to them), but now $\partial f/\partial t$ is modeled using equation (4) [*Trakhtengerts et al*., 2004]. Values of $T_\perp/T_\parallel$ are indicated on each curve. The horizontal line in Figure 8b depicts $(\partial f/\partial t)_{obs}$ for this time.

3. Summary and Conclusions

[18] We have presented examples of chorus emission observed near the equator of Saturn. These emissions are obtained as the spacecraft passes along a high-inclination orbit and a near-constant L-shell when near the magnetic equator. The observations indicate that chorus emission spectral densities are strongest and the emission has the highest bandwidth a few degrees north and south of the magnetic equator. Nearest the magnetic equator the chorus intensities are weaker and the bandwidth is smaller. We speculate that the reason the maximum frequency of the chorus decreases at the highest latitudes is due to propagation effects [cf. *Li et al*., 2011], but this question should be more fully investigated. Within the region of strong chorus emission, nonlinear, frequency-drifting fine structure is observed. We have measured the rate of frequency drift or frequency sweep rate, and compared it to the theory of *Omura et al*. [2008, 2009] and to the theory of *Trakhtengerts* [1999]. Using measured values of B_w, and fitted values of $v_{||}$ and $T_\perp/T_{||}$, we find $(\partial f/\partial t)_O$ derived from equation (3) and the theory of *Omura et al*. [2008] is ~23%–68% of the observed drift rate, $(\partial f/\partial t)_{obs}$. Allowing for a relaxation of the observed electron distribution, with $B_w \sim 2(B_w)_{obs}$ and/or $T_\perp/T_{||} \sim 2\ (T_\perp/T_{||})_{obs}$, the calculated values of $(\partial f/\partial t)_{obs}$ fall within the range of observed values. The values of drift rate calculated from equation (4) of the BWO theory appear to be consistently too low by a factor of at least 2 compared to the values of $(\partial f/\partial t)_O$ for the same plasma parameters. However, in Figure 8 we see that $(\partial f/\partial t)_{Tr}$ does approach $(\partial f/\partial t)_{obs}$ when both B_w and $T_\perp/T_{||}$ are near the limit of the range considered reasonable.

[19] Our results support the nonlinear theory of chorus wave growth allowing for a range of observed plasma parameters as is expected for relaxed electron phase space distributions that have interacted with plasma waves. In addition, we find that there is a distinct region of weaker (linear) chorus growth nearest to the magnetic equator at Saturn.

[20] **Acknowledgments.** We wish to thank J. Barnholdt for administrative assistance and J. Chrisinger for help with several plots. We thank A. Coates and P. Schippers for the electron phase space distributions used in this paper. J.D.M. acknowledges support from JPL contract 1415150 and NASA grant NNX11AM36G. YK is supported by Grant-in-Aid for Young Scientists A (22684025) of the Ministry of Education, Culture, Sports, Science and Technology in Japan, and by the Global COE program "Global Education and Research Center for Earth and Planetary Dynamics" of Tohoku University.

References

Bevington, P. R. (1969), *Data Reduction and Error Analysis for the Physical Sciences*, pp. 113–119, McGraw-Hill, New York.

Bortnik, J., R. M. Thorne, and U. S. Inan (2008), Nonlinear interaction of energetic electrons with large amplitude chorus, *Geophys. Res. Lett.*, *35*, L21102, doi:10.1029/2008GA035500.

Cully, C. M., V. Angelopoulos, U. Auster, J. Bonnell, and O. Le Contel, (2011), Observational evidence of the generation mechanism for rising-tone chorus, *Geophys. Res. Lett.*, *38*, L01106, doi:10.1029/2010GL045793.

Helliwell, R. A. (1967), A Theory of Discrete VLF Emissions from the Magnetosphere, *J. Geophys. Res.*, *72*(19), 4773–4790, doi:10.1029/JZ072i019p04773.

Hospodarsky, G. B., T. F. Averkamp, W. S. Kurth, D. A. Gurnett, J. D. Menietti, O. Santolik, and M. K. Dougherty (2008), Observations of chorus at Saturn using the Cassini Radio and Plasma Wave Science instrument, *J. Geophys. Res.*, *113*, A12206, doi:10.1029/2008JA013237.

Hospodarsky, G. B., J. S. Leisner, K. Sigsbee, J. D. Menietti, W. S. Kurth, D. A. Gurnett, K. A. Kletzing, and O. Santolik (2012), Plasma wave observations at Earth, Jupiter, and Saturn, in *Dynamics of the Earth's Radiation Belts and Inner Magnetosphere*, *Geophys. Monogr. Ser.*, *199*, edited by D. Summers, I. R. Mann, D. N. Baker, and M. Schulz, pp. 415–430, AGU, Washington, D. C.

Katoh, Y., and Y. Omura (2004), Acceleration of relativistic electrons due to resonant scattering by whistler mode waves generated by temperature anisotropy in the inner magnetosphere, *J. Geophys. Res.*, *109*, A12214, doi:10.1029/2004JA010654.

Katoh, Y., and Y. Omura (2006a), Simulation study on nonlinear frequency shift of narrow band whistler mode waves in a homogeneous magnetic field, *Earth Planets Space*, *58*, 1219–1225.

Katoh, Y., and Y. Omura (2006b), A study of generation mechanism of VLF triggered emission by self-consistent particle code, *J. Geophys. Res.*, *111*, A12207, doi:10.1029/2006JA011704.

Katoh, Y., and Y. Omura (2007a), Computer simulation of chorus wave generation in the Earth's inner magnetosphere, *Geophys. Res. Lett.*, *34*, L03102, doi:10.1029/2006GL028594.

Katoh, Y., and Y. Omura (2007b), Relativistic particle acceleration in the process of whistler-mode chorus wave generation, *Geophys. Res. Lett.*, *34*, L13102, doi:10.1029/2007GL029758.

Katoh, Y., and Y. Omura (2011), Amplitude dependence of frequency sweep rates of whistler mode chorus emissions, *J. Geophys. Res.*, *116*, A07201, doi:10.1029/2011JA016496.

Li, W., R. M. Thorne, J. Bortnik, Y. Y. Shprits, Y. Nishimura, V. Angelopoulos, C. Chaston, O. Le Contel, and J. W. Bonnell (2011), Typical properties of rising and falling tone chorus waves, *Geophys. Res. Lett.*, *38*, L14103, doi:10.1029/2011GL047925.

Macúšová, E., et al. (2010), Observations of the relationship between frequency sweep rates of chorus wave packets and plasma density, *J. Geophys. Res.*, *115*, A12257, doi:10.1029/2010JA015468.

Menietti, J. D., O. Santolik, A. M. Rymer, G. B. Hospodarsky, A. M. Persoon, D. A. Gurnett, A. J. Coates, and D. T. Young (2008a), Analysis of plasma waves observed within local plasma injections seen in Saturn's magnetosphere, *J. Geophys. Res.*, *113*, A05213, doi:10.1029/2007JA012856.

Menietti, J. D., O. Santolik, A. M. Rymer, G. B. Hospodarsky, D. A. Gurnett, and A. J. Coates (2008b), Analysis of plasma waves observed in the inner Saturn magnetosphere, *Ann. Geophys.*, *26*, 2631–2644, doi:10.5194/angeo-26-2631-2008.

Menietti, J. D., Y. Y. Shprits, R. B. Horne, E. E. Woodfield, G. B. Hospodarsky, and D. A. Gurnett (2012), Chorus, ECH, and Z mode emissions observed at Jupiter and Saturn and possible electron acceleration, *J. Geophys. Res.*, *117*, A12214, doi:10.1029/2012JA018187.

Nunn, D., Y. Omura, H. Matsumoto, I. Nagano, and S. Yagitani (1997), The numerical simulation of VLF chorus and discrete emissions observed on the Geotail satellite using a Vlasov code, *J. Geophys. Res.*, *102*(A12), 27,083–27,097, doi:10.1029/97JA02518.

Omura, Y., and D. Summers (2004), Computer simulations relativistic whistler-mode wave-particle interactions in the magnetosphere, *Phys. Plasmas*, *11*, 3530–3534, doi: 10.1063/1.1757457.

Omura, Y., and D. Summers (2006), Dynamics of high-energy electrons interacting with whistler mode chorus emissions in the magnetosphere, *J. Geophys. Res.*, *111*, A09222, doi:10.1029/2006JA011600.

Omura, Y., N. Furuya, and D. Summers (2007), Relativistic turning acceleration of resonant electrons by coherent whistler mode waves in a dipole magnetic field, *J. Geophys. Res.*, *112*, A06236, doi:10.1029/2006JA012243.

Omura, Y., Y. Katoh, and D. Summers (2008), Theory and simulation of the generation of whistler-mode chorus, *J. Geophys. Res.*, *113*, A04223, doi:10.1029/2007JA012622.

Omura, Y., M. Hikishima, Y. Katoh, D. Summers, and S. Yagitani (2009), Nonlinear mechanisms of lower-band and upper-band VLF chorus emissions in the magnetosphere, *J. Geophys. Res.*, *114*, A07217, doi:10.1029/2009JA014206.

Santolik, O., D. A. Gurnett, and J. S. Pickett, M. Parrot, and N. Cornilleau-Wehrlin (2003), Spatio-temporal structure of storm-time chorus, *J. Geophys. Res.*, *108*(A7), 1278, doi:10.1029/2002JA009791.

Santolik, O., D. A. Gurnett, J. S. Pickett, J. Chum, and N. Cornilleau- Wehrlin (2009), Oblique propagation of whistler mode waves in the chorus source region, *J. Geophys. Res.*, *114*, A00F03, doi:10.1029/2009JA014586.

Santolik, O., et al. (2010), Wave-particle interactions in the equatorial source region of whistler-mode emissions, *J. Geophys. Res.*, *115*, A00F16, doi:10.1029/2009JA015218.

Summers, D., and Y. Omura (2007), Ultra-relativistic acceleration of electrons in planetary magnetospheres, *Geophys. Res. Lett.*, *34*, L24205, doi:10.1029/2007GL032226.

Tao, X., W. Li, J. Bortnik, R. M. Thorne, and V. Angelopoulos (2012), Comparison between theory and observation of the frequency sweep rates of equatorial rising tone chorus, *Geophys. Res. Lett.*, *39*, L08106, doi:10.1029/2012GL051413.

Titova, E, A. Demekhov, B. Kozelov, O. Santolik, E. Macusova, J.-L. Rauch, J.-G. Trotignon, D. Gurnett, and J. Pickett (2012), Properties of the magnetospheric

backward wave oscillator inferred from CLUSTER measurements of VLF chorus elements, *J. Geophys. Res.*, *117*, A08210, doi:10.1029/2012JA017713.

Trakhtengerts, V. Y., M. J. Rycroft, and A. G. Demekhov (1996), Interrelation of noise-like and discrete ELF/VLF emissions generated by cyclotron interactions, *J. Geophys. Res.*, *101*(A6), 13,293–13,301, doi:10.1029/95JA03515.

Trakhtengerts, V. Y. (1999), A generation mechanism for chorus emission, *Ann. Geophys.*, *17*, 95–100, doi:10.1007/s00585-999-0095-4.

Trakhtengerts, V. Y., A. G. Demekhov, E. E. Titova, B. V. Kozelov, O. Santolik, D. Gurnett, and M. Parrot (2004), Interpretation of Cluster data on chorus emissions using the backward wave oscillator model, *Phys. Plasmas*, *11*(4), 1345–1351, doi: 10.1063/1.1667495.